Journal of Applied Research and Technology

www.jart.icat.unam.mx

Journal of Applied Research and Technology 24 (2026) 632-641

Original

Investigating the Impact of the Open-Ended Coaxial Sensor Design on the Reflection Coefficient Using the Method of Moments

Hojjatollah Soleimani[1] • Surajudeen Sikiru[3*]
Hassan Soleimani[2] • Zulkifly Abbas[4]

[1]*Department of Physics, North Tehran Branch, Islamic Azad University, 16511-53311, Tehran, Iran.*
[2]*School of Physics and Materials Studies, Faculty of Applied Sciences, Universiti Teknologi Mara, 40450, Shah Alam, Selangor, Malaysia.*
[3]*Geoscience Department, Universiti Teknologi PETRONAS, Seri Iskandar 32610, Perak, Malaysia.*
[4]*Department of Electrical and Electronics Engineering, Xiamen University, Malaysia.*

Received 10 27 2024; accepted 11 25 2024
Available 10 31 2025

Abstract: Reflection coefficient measurements are critical and widely used to determine the permittivity and moisture content of materials. The calculation of both the magnitude and phase of an open-ended coaxial reflection coefficient via the Method of Moments (MoM) is presented. The solution to the problem of calculating the reflection coefficient of the PTFE-filled coaxial sensor for air is obtained by converting the electric field integral equations into a linear system. The variation of the measured and calculated magnitude reflection coefficient as a function of frequency for air at room temperature was found to be 0.7 to 1.02. A comparison between MoM and the quasi-static method, using measured data, showed that MoM was closer to the measured magnitude. The phase reflection coefficient was also more accurate with MoM than with the quasi-static method. The calculation of the reflection coefficient using analytical (quasi-static) and numerical (MoM) methods for air as the sample was shown to compare favorably with the measured magnitude and phase of the reflection coefficient.

Keywords: Reflection coefficient; Method of Moments, permittivity, open-ended coaxial, quasi-static

*Corresponding author.
E-mail address: surajudeen86@gmail.com (B. Nazar).
Peer Review under the responsibility of Universidad Nacional Autónoma de México.

1. Introduction

One of the most extensively used sensors for determining the dielectric characteristics of materials at microwave frequencies is the open-ended coaxial approach. Using the analytical admittance model (Soleimani, 2010, Levine and Papas, 1951; Soleimani et al., 2024). The permittivity of the material under test is typically determined from the observed reflection coefficient. Unfortunately, the analytical solutions are incorrect due to the formulations' assumptions of homogeneity, such as the use of an approximate technique to handle the singularity in the equations (Soleimani, 2010). Several computational strategies have been developed to handle electromagnetic (EM) issues that do not lend themselves to analytical or precise solutions (Šarolić & Matković, 2022; Yusuf et al., 2021). The Method of Moments (MoM), the Finite Element Method (FEM), and the Finite Difference Time Domain (FDTD) method are the most commonly used approaches. For the derivation of governing equations, FEM is more suitable for irregular wave problems than MoM, as a comparison of the two procedures outlined in the preceding paragraph. FEM is a useful approach; however, the primary issue is that human preparation and program execution time exceed that of MoM. The MoM is the most suitable solution for addressing open-boundary issues; however, it is significantly more difficult than FEM in terms of overall operations. In tackling integral-based electromagnetic issues, R.F. developed the Method of Moments (MoM) (Dilman et al., 2023; Gibson, 2021; Soleimani et al., 2023). Since then, it has been widely utilized, and numerous fast algorithms based on the Method of Moments have been devised (Chew et al., 2001).

In recent years, open-ended coaxial wires have been widely used as sensors to detect the permittivity of biological molecules (Sutthaweekul, 2019). Due to their uncomplicated design and compact size (with the possibility of being as small as 0.5 mm in diameter), these sensors' equivalent circuit characteristics were determined either through direct measurements or by inference from tests conducted on known dielectrics using the lumped circuit approach. Additionally, the fringing capacitances were presumed to be directly proportional to the permittivity (ε) and to remain unaffected by the signal frequency (Yusuf et al., 2020; Yahya et al., 2020). The objective of this study is to employ numerical methods to examine how the fringing capacitance of coaxial sensors varies with the sample permittivity, as depicted in Fig. 1. The focus is on investigating the two-capacitance, or linear, model, which relates the net fringing capacitance to the sample permittivity. As it is well established (Suhaime, 2018) that the fringing capacitance remains constant from direct current (dc) to microwave frequencies in the case of a homogeneous scenario (for all practical line widths), this research focuses solely on estimating static fringing capacitances.

To address the static conductor-dielectric problems at hand, both the Finite Element Method (FEM) and the Method of Moments (MoM) were applied, employing a set of interconnected integral equations (Bisgaard, 2000; Meziat et al., 2007). Only a lossless dielectric is modeled since all solutions are static. The application works on the premise that a reflected signal through the coaxial aperture will contain the necessary information about the material sample at the terminal surface. As a result, if the aperture admittance or reflection coefficient features are accurately defined, they may be utilized as a probe to characterize material samples. Nonetheless, no fully analytical link exists between the reflection coefficient and the permittivity of the material under examination.

2. Vector Moment Method Analysis of an Open-Ended Coaxial Line

2.1 Partial Difference Equation

An open-ended coaxial line is made up of an inner and outer conductor with radii *a* and b. Figure 1 depicts the Infinity. Maxwell's equation provides the partial differential equation (PDE) formulation for any TM wave:

$$\left(\nabla \times \vec{H}\right) = (\sigma + j\omega\varepsilon)\vec{E} \tag{1}$$

$$\left(\nabla \times \vec{H}\right) = (\vec{J} + \frac{\varepsilon\,\partial \vec{E}}{\partial t}) \tag{2}$$

Where $\varepsilon = \varepsilon_0\varepsilon_r$ is the permittivity of the material. For the open coaxial line, the magnetic field, $\vec{\boldsymbol{H}}$ is a function of $\boldsymbol{\rho}$ and $\boldsymbol{z}$ but independent of $\boldsymbol{\phi}$, thus

$$-\frac{\partial}{\partial \rho}\left(\frac{1}{\varepsilon\rho}\frac{\partial}{\partial \rho}\left(\rho H_\phi\right)\right) - \frac{1}{\varepsilon}\frac{\partial^2}{\partial Z^2}H_\phi - \mu k_0^2 H_\phi = 0 \tag{3}$$

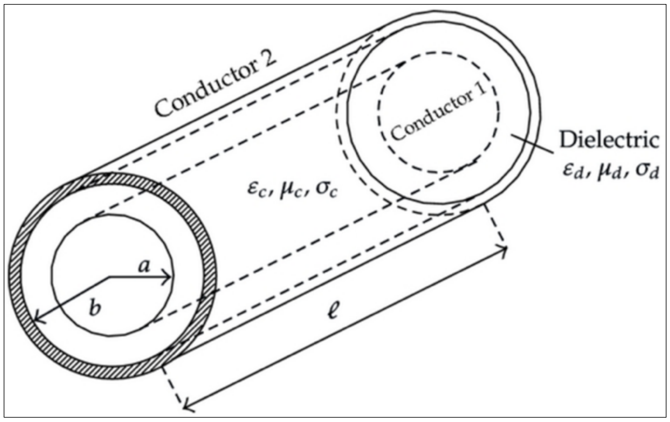

Figure 1: Coaxial line.

We can find an equation for the aperture surface of the coaxial line, $E_\rho(\rho, 0)$ is the radial electric field intensity over the aperture. The following is the magnetic field intensity Type equation. The equation for the medium over the ground plane, which is a linear, isotropic, homogeneous, nonmagnetic substance with complex permittivity, is as follows:

$$H^{+}{}_{\phi}(\rho,0) = \frac{j\omega\varepsilon_0\varepsilon}{\pi}\int_a^b E_\rho(\rho',0)\rho' \int_0^\pi \frac{\cos(\phi')\exp(-jkr)}{r} d\phi' d\rho' \quad (4)$$

$$\text{If } z = 0 \qquad r^2 = \rho^2 + \rho'^2 - 2\rho\rho'\cos(\phi')$$

For an internal coaxial line with the field component inside the line, z < 0 is expressed in terms of the forward traveling fundamental TEM mode, its reflection at the interface, and a series of TM evanescent modes generated at the discontinuity. In general, the field in the coaxial line is expressed as:

$$H^{-}{}_{\phi}(\rho,0) = \frac{1}{\pi\rho} + j\omega\varepsilon_0\varepsilon_l\int_a^b E_\rho(\rho',0)K_C(\rho,\rho')\rho' d\rho' \quad (5)$$

Where ε_l is the permittivity of the coaxial line.?

Thus: $$\boldsymbol{K_C}(\rho,\rho') = j\sum_{n=0}^{\infty}\frac{\Phi_n(\rho)\Phi_n(\rho')}{A_n^2\beta_n} \quad (6)$$

$$\Phi_n(\rho) = [Y_0(\gamma_n a)J_1(\gamma_n\rho) - J_0(\gamma_n a)Y_1(\gamma_n\rho)] \quad (7)$$

$$\Phi_n(\rho') = [Y_0(\gamma_n a)J_1(\gamma_n\rho') - J_0(\gamma_n a)Y_1(\gamma_n\rho')] \quad (8)$$

$$A_n^2 = \frac{2}{\pi^2\gamma_n^2}\left[\frac{J_0^2(\gamma_n a)}{J_0^2(\gamma_n b)} - 1\right] \qquad n \geq 1 \quad (9)$$

$$\beta_n = \begin{cases} \sqrt{(k_l^2-\gamma_n^2)}, & k_l > \gamma_n \\ -j\sqrt{(\gamma_n^2-k_l^2)}, & k_l < \gamma_n \end{cases} \quad (10)$$

$$\beta_0 = k_l \qquad \gamma_0 = 0 \qquad A_0^2 = \mathrm{Ln}\left(\frac{b}{a}\right) \quad (11)$$

J_n and Y_n are Bessel functions of the first and second kinds of order n, respectively. The γ_n are solutions to the following characteristic equation:

$$Y_0(\gamma_n a)J_0(\gamma_n b) = J_0(\gamma_n a)Y_0(\gamma_n b) \quad (12)$$

According to two different coaxial lines, internal and aperture fields, we can observe that when z=0, then two variety fields, H^+ and H^-, are equal. Thus, these equations are studied:

$$\frac{1}{\pi\rho} + j\omega\varepsilon_0\varepsilon_l\int_a^b E_\rho(\rho',0)\boldsymbol{K_C}(\rho,\rho')\rho' d\rho' = \frac{j\omega\varepsilon_0\varepsilon}{\pi}\int_a^b E_\rho(\rho',0)\rho'\int_0^\pi\frac{\cos(\phi')\exp(-jkr)}{r}d\phi' d\rho' \quad (13)$$

Thus:

$$\int_a^b E_\rho(\rho',0)\left(\rho'\varepsilon\int_0^\pi\frac{\cos(\phi')\exp(-jkr)}{r}d\phi' - \rho'\pi\varepsilon_0\varepsilon_l K_C(\rho,\rho')\right) d\rho' = \frac{1}{j\omega\rho} \quad (14)$$

Where **j**: imaginary unit, where $j^2 = -1$; it represents the complex phase factor used in the context of wave propagation. **ω**: angular frequency of the wave, related to the frequency *f* of the wave by $\omega = 2\pi f$. ε_0: permittivity of free space (vacuum permittivity), which is a fundamental physical constant; it represents the ability of a vacuum to permit electric field lines. ε: the relative permittivity (dielectric constant) of the material inside the coaxial line or system; it represents the ratio of the permittivity of the material to the permittivity of free space ($\varepsilon=\varepsilon_r$). ρ' : radial coordinate, $E\rho(\rho',0)$; this represents the electric field in the radial direction (ρ direction) at some point (ρ') in the coaxial line or system. The field is evaluated at z=0, suggesting that it may be evaluated at the surface or another reference point.

To transform integral equations into a matrix equation, the Method of Moments [3] is extensively utilized. A linear operator equation can also be converted to a matrix equation. The following is an example of a linear operator equation:

$$\boldsymbol{L} \times \boldsymbol{f} = \boldsymbol{g} \qquad (15)$$

Where $\boldsymbol{L}$ is a linear operator, $\boldsymbol{f}$ is the unknown function responding to excitation $\boldsymbol{g}$. The unknown function f is expanded in terms of a set of essential functions, namely:

$$f = \sum_{n=1}^{N} a_n f_n \qquad (16)$$

The problem now becomes finding a_n. Substituting (15) into (16), we have:

$$\sum_{n=1}^{N} a_n L f_n = g \qquad (17)$$

Multiplying the above by W_m, which serves as a testing function, we arrive at a matrix equation or, more specifically:

$$[w_{mn}].[a_n] = [g_m] \qquad (18)$$

Where the elements of W_{mn} and $\mathbf{g_m}$ are known, and $\mathbf{a_n}$ is the unknown column vector. Then, $\mathbf{a_n}$ is evaluated as follows:

$$[a_n] = [w_{mn}]^{-1}.[g_m] \qquad (19)$$

Once a matrix equation is given, various methods can be used to solve for the unknown coefficients. The most straightforward and reliable process in our later calculation was decomposition. Many iterative solvers and fast algorithms can be applied to speed up calculation (Liu et al., 2010).

We can separate Equation (14), and it can be written according to the following matrices:

$$[g_{m,m2}] = \frac{1}{j\omega\rho_{m1m2}} \qquad (20)$$

$$[a_n] = \int_a^b E_\rho(\rho', 0)\,d\rho' \qquad (21)$$

$$[w_{m,n}] = (\rho' \, \varepsilon \int_0^\pi \frac{\cos(\phi')\exp(-jkr)}{r} d\phi' - \rho' \, \pi\varepsilon_0\varepsilon_l K_C(\rho_m, \rho_n')) \qquad (22)$$

Give

$$K_{1c} = \int_0^\pi \frac{\cos(\phi')\exp(-jkr)}{r} d\phi' \qquad (23)$$

$$\text{If } \rho^2 \neq \rho'^2 \rightarrow K_{1c} = \sum_0^{180} \frac{\cos(\phi')\exp(-jkr)}{r} \qquad (24)$$

$$\text{If } \rho^2 = \rho'^2 \rightarrow K_{1c} = \sum_{0.1}^{180} \frac{\cos(\phi')\exp(-jkr)}{r} \qquad (25)$$

The following equation produces the m=N equation of the form $\sum_{n=1}^{N} w_{mn} a_n = \frac{1}{j\omega\rho_m} \quad m = 1,2,\dots,N$

According to the following equation, we can approximate the aperture admittance (Xu et al., 1991):

$$Y_l = \frac{2}{\int_a^b E_\rho(\rho',0)d\rho'} - \frac{2\pi}{\mathrm{Ln}(\frac{b}{a})\sqrt{\frac{\mu_0}{\varepsilon_0\varepsilon_l}}} \qquad (26)$$

The admittance charge of the coaxial line (27), normalized aperture admittance (28), and reflection coefficient (29) are calculated as follows (Pournaropoulos & Misra, 1994):

$$Y_0 = \frac{2\pi}{\mathrm{Ln}(\frac{b}{a})\sqrt{\frac{\mu_0}{\varepsilon_0\varepsilon_l}}} \qquad (27)$$

$$\tilde{Y} = \frac{Y_l}{Y_0} \qquad (28)$$

$$S_{11} = \frac{1-\tilde{Y}}{1+\tilde{Y}} \qquad (29)$$

The ground plane is divided into M concentric annular zones of coaxial sensor width (Figure 2).

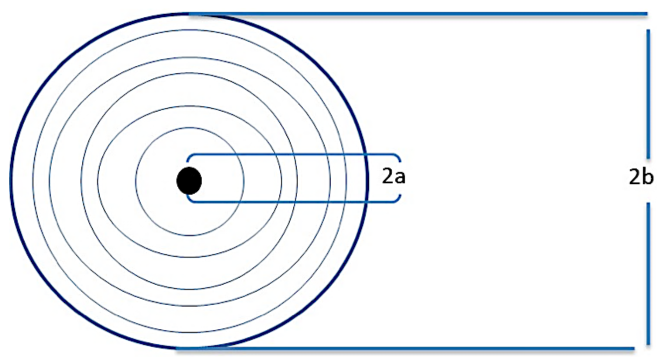

Figure 2. Ground plane with annular zones surface coaxial sensor.

3. Results and Discussion

The variation of the measured and calculated | Γ | with frequency for air at room temperature is shown in Figures 3a and 3b. The | Γ | varies in the range of 0.7 to 1. Even though it shows fluctuations, the value can still be approximated as 1. It can be observed that the compared value is similar to the calculated | Γ |, which is obtained from the quasi-static method and MoM. This fluctuation may be due to the multiple reflections in the measurement. The magnitude is strongly affected by the mismatch impedance.

Meanwhile, the mismatch impedance depends on the sample permittivity. Therefore, the nearly constant magnitude is due to the invariant dielectric constant and loss factor of air as the frequency varies (Figure 3c). The phase is a function of sample thickness and permittivity. As mentioned previously, the dielectric and loss factors are constant when the frequency varies. However, this variation is insignificant, as the negative phase goes from 0 rad to -0.1 rad.

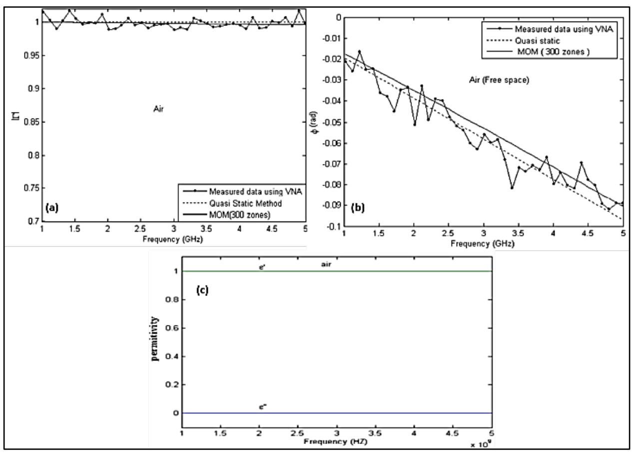

Figure 3. Variation in reflection coefficient with frequency for air: (a) magnitude, (b) phase, and (c) variation in dielectric constant and loss factor with frequency at room temperature for air.

The accuracy of MoM and the quasi-static method in magnitude and phase can be reviewed; magnitudes obtained from the quasi-static method may be observed to fluctuate with frequency, as shown in Figure 4(a). The trendline's fluctuations are around 0.0092, even though valor absoluto de incremento mayúscula gamma , final valor absoluto subíndice mayúscula M o mayúscula M varies with increasing frequencyequency increases. By comparing the magnitude of MoM and the quasi-static method, it can be found that MoM agrees better with the measured magnitude. This can be proved by comparing mean $|\Delta\Gamma|_{MoM}$ and $|\Delta\Gamma|_{quasi}$. The comparison reveals that MoM shows a smaller $|\Delta\Gamma|$than the quasi-static method ($|\Delta\Gamma|_{quasi}$ = 0.0593).

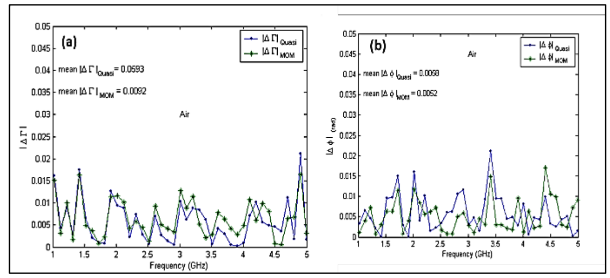

Figure 4. Variation in (a) $|\Delta\Gamma|$ and (b) $|\Delta\Phi|$ with frequency for air.

By removing the second term from (27), the frequency-independent component of the capacitance of the coaxial opening may be calculated. The capacitance thus obtained is divided by C_0 (b – a) for a cable with b/a = 3.27 and ε_0= 2.05. The variation of the measured and calculated | Γ | with frequency for air at room temperature is shown in Figure 3. The | Γ | varies in the range of 0.7 to 1.02. Even though it shows fluctuations, the value can still be approximate as 1. It is observed that this approximate value is similar to the calculated | Γ | obtained using the quasi-static method and MoM. This fluctuation may be due to multiple reflections in the measurement. The magnitude is strongly affected by the mismatch impedance. Meanwhile, the mismatch impedance is the function of the permittivity of the medium. Therefore, constant magnitude exists due to the invariant dielectric constant and loss factor for air when frequency varies.

The phase is a function of the medium's thickness and permittivity. As mentioned previously, the dielectric and loss factors are constant when the frequency varies. However, this variation is insignificant; the negative phase varies from 0 rad to -0.1 rad. The accuracy of MoM and quasi-static in magnitude and phase can be reviewed in Figure 4. It can be observed that $|\Delta\Gamma|_{quasi}$- increases with frequency, as shown in Figure 4(a). There is a fluctuating trendline due to the fluctuations in the measured results. However, the $|\Delta\Gamma|_{MOM}$ seems to be constant at 0.0092 even though $|\Delta\Gamma|_{MOM}$ fluctuates when frequency increases. Comparing the magnitude of MoM and the quasi-static method determines that MoM is closer to the measured magnitude. This can be demostrated by comparing mean $|\Delta\Gamma|_{MOM}$ and $|\Delta\Gamma|_{quasi}$. The comparison reveals that MoM shows a smaller $|\Delta\Gamma$ than the quasi-static method ($|\Delta\Gamma|_{quasi}$ = 0.0593). The variation of $|\Delta\Phi|_{quasi}$ and $|\Delta\Phi|_{MOM}$ with frequency seems similar when they fluctuated within a similar range of $|\Delta\Phi|$, that is, from 0 to 0.05 rad, as shown in Figure 4 (b). The mean $|\Delta\Phi|_{quasi}$ is similar to $|\Delta\Phi|_{MOM}$, and their value is listed in Figure 4 (b).

The variation of $|\Gamma|$ with frequency measured at room temperature for water is shown in Figure 5(a). $|\Gamma|$ decreases from 0.97 to 0.78 with increasing frequency. Figure 5 shows that it decreases when frequency increases. Meanwhile, it increases when the frequency increases. This behavior affects the $|\Gamma|$ directly. Consequently, the $|\Gamma|$ decreases when frequency increases, as shown in Figure 5(a). The greater value of ε'' is obtained when frequency increases if compared with ε''. It implies that the energy stored in the water at room temperature is more significant than energy dissipation. It can be illustrated in Figure 5 where ε' is much higher than ε'. Water has a higher tendency to store energy than to dissipate it. ε' is more significant than in complex permittivity for water. The impedance of water decreases frequently. Hence, the mismatch impedance decreases as well. This phenomenon causes the $|\Gamma|$ and Φ to decrease when frequency increases.

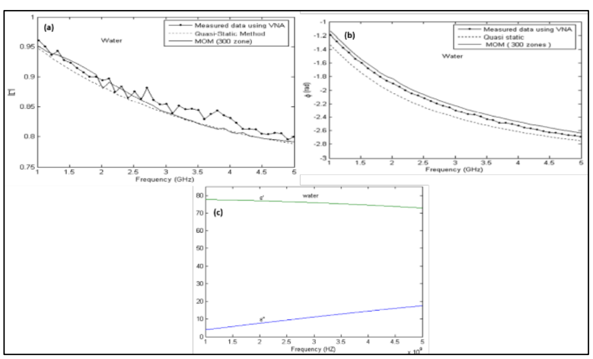

Figure 5: Variation in reflection coefficient with frequency for water: (a) magnitude Γ and (b) phase ϕ, and (c) The variation in dielectric constant and loss factor with frequency at room temperature for water.

In Figure 6(a), it can be observed that $|\Delta\Gamma|$ fluctuates when frequency increases. $|\Delta\Gamma|_{MOM}$ decreases to 3.1 GHz and then increases water ionic polarization at this frequency. Meanwhile, $|\Delta\Phi|_{quasi}$ has a peak at about 3.25 GHz. This implies that MoM shows the most accurate results at 3.2G Hz. This peak is smaller than the peak presented by the quasi-static method ($|\Delta\Phi|_{quasi}$). For frequency less than 2.9 GHz, $|\Delta\Phi|_{quasi}$ is higher than $|\Delta\Gamma|_{MOM}$. When the frequency exceeds 2.9 GHz, $|\Delta\Phi|_{quasi}$ is slightly smaller than $|\Delta\Gamma|_{MOM}$. Therefore, the mean $|\Delta\Gamma|_{MOM}$ has a smaller value than $|\Delta\Phi|_{quasi}$, that is, 0.0072 rad and 0.0130 rad, respectively. This is similar to the case of magnitude for air. Similarly, the phase condition is similar to a magnitude where mean $|\Delta\Gamma|_{MOM}$ is smaller than $|\Delta\Phi|_{quasi}$. From Figure 6(b), this can be observed that $|\Delta\Gamma|_{MOM}$ = 0.0492 rad and $|\Delta\Phi|_{quasi}$ = 0.0948 rad. From Figure 6(b), $|\Delta\Phi|_{quasi}$ decreases with increasing frequency. Meanwhile, $|\Delta\Gamma|_{MOM}$ constantly fluctuates at about 0.0492 rad. However, the quasi-static method performs better at low frequencies than at high frequencies.

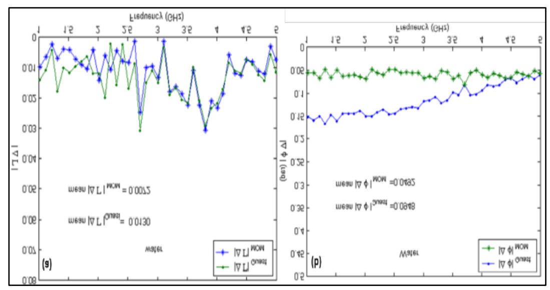

Figure 6: The variation in (a) $|\Delta\Gamma|$ and (b) $|\Delta\Phi|$ with frequency at room temperature for water.

The variation of the measured $|\Gamma|$ with frequency at room temperature for propanol is shown in Figure 7. The measured and calculated magnitude (MoM and the quasi-static method) has a similar trendline as in the case of water. The magnitude decreases with increasing frequency. The phase is similar to a magnitude where the phase decreases with increasing frequency. From Figure 7c, it can be observed that and is almost the same at 1.5 GHz. When the frequency exceeds 1.5 GHz, they start to diverge from each other. Increases exponentially and tends to become constant.

Meanwhile, it decreases exponentially. However, the value is still higher than when the frequency exceeds 1.5 GHz. The fluctuation of magnitude in Figure 7 (a) seems more severe than the phase in Figure 7 (b).

This causes the mean phase error shown in Figure 8(b) to experience severe fluctuation. For propanol, MoM works differently from the other sample, where the MoM ($|\Delta\Gamma|_{MOM}$) shows a more significant mean magnitude error when compared with the quasi-static method ($|\Delta\Phi|_{quasi}$). The $|\Delta\Gamma|_{MOM}$ and $|\Delta\Phi|_{quasi}$ is 0.0175 and 0.0288, respectively. However, $|\Delta\Phi|_{MoM}$ has unlike condition as from the magnitude in Figure 8(b) because $|\Delta\Gamma|_{MOM}$ is smaller than $|\Delta\Phi|_{quasi}$. $|\Delta\Phi|_{MoM}$ and $|\Delta\Phi|_{quasi}$ is 0.0260 rad and 0.0512 rad, respectively. The quasi-static method is more accurate than the MoM method for propanol in terms of magnitude.

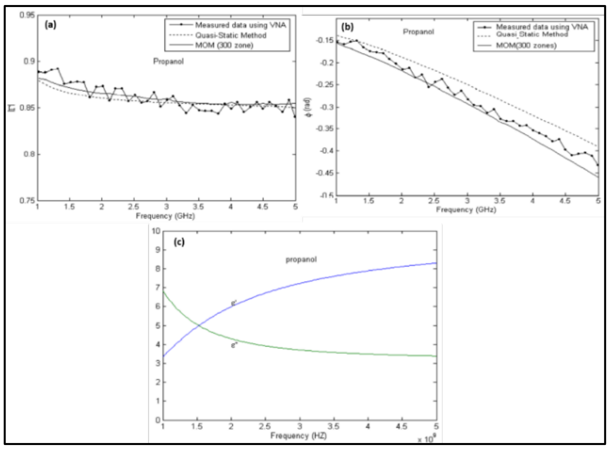

Figure 7: Variation in reflection coefficient with frequency for propanol: (a) magnitude $|\Gamma|$, (b) phase ϕ, and (c) the variation in dielectric constant and loss factor with frequency at room temperature for propanol.

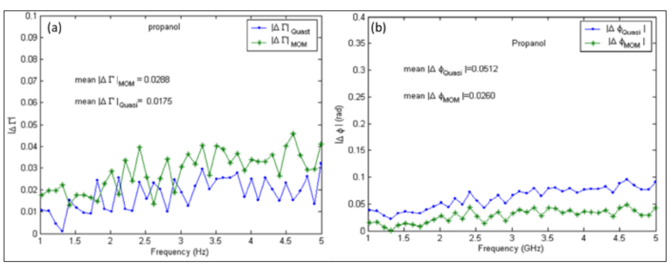

Figure 8: The variation in (a) ($|\Delta\Gamma|$ and (b) $|\Delta\Phi|$ with frequency at room temperature for propanol.

The variation of the measured $|\Gamma|$ with frequency at room temperature for ethanol is shown in Figures 9(a) and b. From Figure 9(c), ε' drops exponentially with increasing frequency and decreases with increasing frequency from 1 to 1.2 GHz. When frequency exceeds 1.2 GHz ε'' starts to increase. Figure 9(c) shows that when frequency increases, the difference between $\varepsilon'$and ε'' decreases gradually.

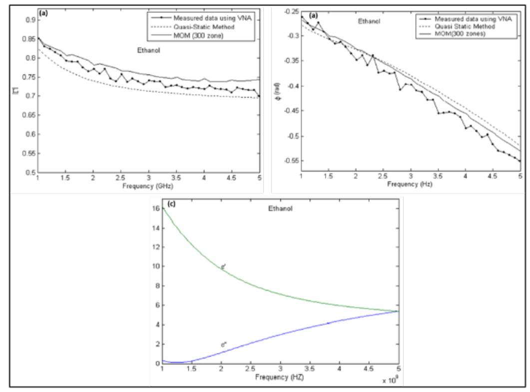

Figure 9: Variation in the reflection coefficient with frequency for ethanol: (a) magnitude $|\Gamma|$ and (b) phase ϕ, (c) the variation in dielectric constant and loss factor with frequency at room temperature for ethanol.

Therefore, the measured magnitude and calculated magnitude (MoM and quasi-static method) decrease exponentially and tend to become constant when frequency increases. Meanwhile, the phase decreases linearly with frequency and increases with frequency $|\Delta\Phi|_{MoM}$ and $|\Delta\Phi|_{quasi}$ their values are 0.0580 and 0.0345 rad, respectively. However, $|\Delta\Phi|_{MoM}$ and $|\Delta\Phi|_{quasi}$ seem constant when frequency increases, with values of 0.0180 and 0.0224 rad, respectively. Their comparisons are visualized in Figure 10. The result of MoM has better agreement with measured results when compared with the quasi-static method.

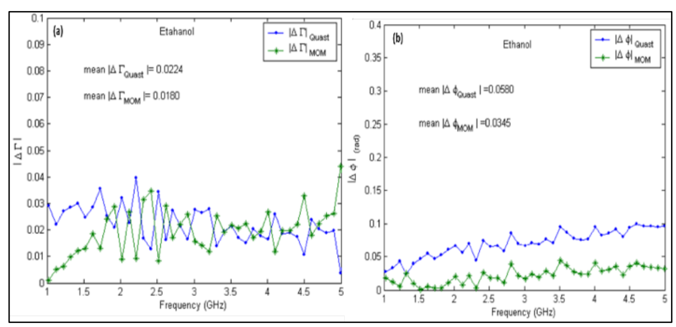

Figure 10: The variation in (a) $|\Delta\Gamma|$ and (b) $|\Delta\Phi|$ with frequency at room temperature for ethanol.

The situation of methanol is similar to ethanol and propanol. The measured and calculated magnitude (MoM and the quasi-static method) have a similar trendline as in the case of ethanol and propanol. The magnitude $|\Gamma|$ and Φ decrease when the frequency varies from 1 GHz to 5 GHz, as shown in Figure 11. From Figure 11(c)), it can be observed that ε' decreases when frequency increases. Meanwhile, ε'' increases from 1 GHz to 2.5 GHz and tends to become constant for frequency higher than 2.5 GHz. Generally, ε' still shows a greater value than ε''.

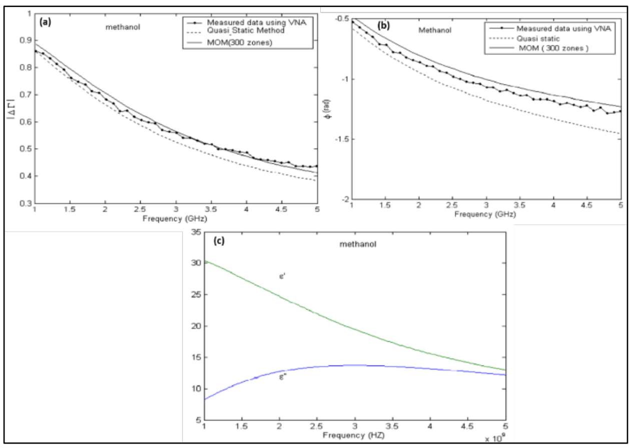

Figure 11: Variation of (a) magnitude $|\Gamma|$ of the reflection coefficient with frequency for methanol: (b) phase ϕ, and (c) the variation in dielectric constant and loss factor with frequency at room temperature for methanol.

The MoM still shows higher accuracy and smaller mean errors in magnitude and phase than the quasi-static method. ($|\Delta\Gamma|_{quasi}$ and $|\Delta\Phi|_{quasi}$ shown in Figure 12(a) and 12(b), are 0.0703 and 0.0937 rad, respectively, as shown in Figure 12(a). Meanwhile, $|\Delta\Gamma|_{MOM}$ and $|\Delta\Phi|_{MoM}$ is 0.0373 and 0.0474 rad, as shown in Figure 12(b).

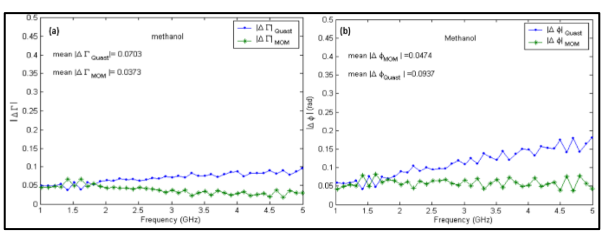

Figure 12 The variation in (a) $|\Delta\Gamma|$ and $|\Delta\Phi|$ (b) with frequency at room temperature for methanol.

As shown in Tables 1 and 2, among all the reference samples (excluding air) discussed previously, MoM achieves the highest accuracy for both magnitude and phase. They show smaller mean $|\Delta\Gamma|$ and $|\Delta\Phi|$ values. This can be demonstrated by comparing their mean $|\Delta\Gamma|$ and $|\Delta\Phi|$. Meanwhile, $|\Delta\Gamma|$ and $|\Delta\Phi|$ of MoM are the smallest for air, namely 0.0042 and 0.0052 rad.

Table 1. Percentage of errors in MoM and quasi-static method with respect to measured data $|\Delta\Gamma|$ and $|\Delta\Phi|$.

Materials	$|\phi_{Measure}-\phi_{MOM}|$	$|\phi_{Measure}-\phi_{Quasi}|$
Air	0.0052	0.0058
Water	0.0492	0.0948
Propanol	0.0260	0.0512
Ethanol	0.0345	0.0580
Methanol	0.0474	0.0937

Materials	$|\Gamma_{Measure}-\Gamma_{MOM}|$	$|\Gamma_{Measure}-\Gamma_{Quasi}|$
Air	0.0042	0.0119
Water	0.0072	0.0130
Propanol	0.0280	0.0175
Ethanol	0.0180	0.0224
Methanol	0.0373	0.0703

Table 2. Comparison MOM with vector network analyzer for 2 GHz frequency.

	VNA		MoM		Different	
	Magnitude	Phase	Magnitude	Phase	Magnitude	Phase
Air	0.9829	-32.57	0.9582	-29.81	0.0247	2.76
Water	0.8841	-116.25	0.9143	-115.30	0.0302	0.95
Ethanol	0.849	-42.52	0.8493	-45.32	0.0002	2.80
Propanol	0.8939	-35.70	0.8890	-35.59	0.0049	0.11
Methanol	0.7403	-82.40	0.7701	-85.54	0.0298	3.14

Moreover, the smaller value of ε' for m.c. less than 35% was due to the lower relaxation frequency of water at all frequencies. Fewer water molecules in the sample (low moisture content) cause the water molecules to be bound and absorbed on the mesocarp surface. Therefore, their mobility is restricted, so the relaxation frequency is lower than that of free water. Due to the low relaxation frequency, polarization may not fully develop for moisture content less than 35%. When the m.c. is higher than 35%, no more water molecules can be adsorbed, and it will become free water (Cheng et al., 2012). The relaxation frequency may become relatively higher than the operating frequency. Hence, the dielectric constant increases when the moisture content increases. Similarly, the loss factor, ε'' is small for moisture content less than 35%. As mentioned previously, the relaxation frequency is low when the moisture content is less than 35%. ε" is directly proportional to the frequency. As frequency increases, water molecules bend and rotate periodically, and friction between them increases.

The loss per cycle is directly proportional to frequency. Meanwhile, friction is directly proportional to the speed of movement (relaxation frequency) in a viscous fluid as in mesocarp because the water molecules are very close to their neighbors. For the case in which the relatively low relaxation frequency is compared with the operating frequency (1–5 GHz), the loss factor seems linear when moisture content is less than 35%. When the moisture contents exceeds 35%, the relaxation frequency increases. The orientation of water molecules still occurs; however, it is also slowed down by friction and causes energy loss during friction. Thus, the loss factor increases when the moisture contents exceeds 35%. To improve the accuracy of the mixture model, calculation of the correct shapes and fields at the particle level in the corn sample is required. Thus, the accuracy of the coaxial sensor can only be determined by comparing the predicted moisture content with the accurate moisture content determined by the oven-drying method.

Conclusion

In this work, the Method of Moments technique has been used to solve the wave equation in the two dimensions of the open-ended coaxial sensor to determine the reflection coefficient of air. The results were closely aligned with measured data found using a vector network analyzer. The conclusions based on the measured results are briefly summarized as follows:

- With the MoM, the designer can test several probe configurations without building them. From the MoM results, the microwave characteristics of the coaxial probe can be predicted.
- The coaxial sensor is sufficient to determine fruit quality based on the measured phase of the reflection coefficient ϕ alone for medium-sized fruit at low frequencies (< 5 GHz).
- MoM is a method with high accuracy and helps calculate the coaxial sensor's reflection coefficient.
- Compare Finite Element Simulation (FEM) results with other numerical techniques, such as the Method of Moments (MoM) and Finite-Difference Time-Domain (FDTD). The reason is to determine which numerical techniques are high-speed, economical and provide accurate simulation results.
- Construct a portable online microwave measurement system to replace the VNA for in-situ measurements. The manufacturer is only interested in low-cost instruments and convenient instrument systems for plantation usage in the industry.
- Investigate in detail (microscopically) other composition properties, such as the dielectric properties and the distribution of water in the mesocarp. This study can additionally be extended to microwave techniques.

Funding

The authors did not receive any sponsorship to conduct the research reported in the present manuscript.

Conflict of interest

The authors do not have any type of conflict of interest to declare.

References

Bisgaard, T. M. (2000). A Method of Moments for Semigroups S without Zero, but Satisfying S = S + S. Semigroup Forum, 61(3), 317–332.
https://doi.org/10.1007/pl00006030

Cheng, E. M., Malek, M. F. B. A., Ahmed, M., You, K. Y., Lee, K. Y., & Nornikman, H. (2012). The use of Dielectric Mixture Equations to analyze the Dielectric Properties of a Mixture of Rubber Tire Dust and Rice Husks in a Microwave Absorber. Electromagnetic Waves, 129, 559–578.
https://doi.org/10.2528/pier12050312

Chew, W.C., Jin, J.-M., Michielssen, E., & Song, J. (2001). Fast Efficient Algorithms in Computational Electromagnetics. Artech.

Dilman, I., Çayören, M., & Akinci, M. N. (2023). Maximum likelihood estimation of debye relaxation parameters with Open-Ended Coaxial probes. IEEE Transactions on Instrumentation and Measurement, 72, 1–8.
https://doi.org/10.1109/tim.2023.3267352

Gibson, W. C. (2021). The method of moments in electromagnetics.
https://doi.org/10.1201/9780429355509

Levine, H., & Papas, C. H. (1951). Theory of the circular diffraction antenna. Journal of Applied Physics, 22(1), 29–43.
https://doi.org/10.1063/1.1699816

Liu, L., Xu, H., Lichtenberger, A. W., & Weikle, R. M. (2010). Integrated 585-GHz Hot-Electron Mixer Focal-Plane arrays based on annular slot antennas for imaging applications. IEEE Transactions on Microwave Theory and Techniques, 58(7), 1943–1951.
https://doi.org/10.1109/tmtt.2010.2050101

Meziat, R., Patiño, D., & Pedregal, P. (2007). An alternative approach for non-linear optimal control problems based on the method of moments. Computational Optimization and Applications, 38(1), 147–171.
https://doi.org/10.1007/s10589-007-9032-1

Pournaropoulos, C., & Misra, D. (1994). A study on the coaxial aperture electromagnetic sensor and its application in material characterization. IEEE Transactions on Instrumentation and Measurement, 43(2), 111–115.
https://doi.org/10.1109/19.293405

Šarolić, A., & Matković, A. (2022). Dielectric permittivity measurement using Open-Ended Coaxial Probe—Modeling and Simulation based on the Simple Capacitive-Load Model. Sensors, 22(16), 6024.
https://doi.org/10.3390/s22166024

Soleimani, H. (2010). Method of Moment Analysis Using Open-ended Coaxial Sensor in Determination of Corn Reflection Coefficient (Doctoral dissertation, Universiti Putra Malaysia).

Soleimani, H. Sikiru, S., Abbas, Z., Soleimani, H., Kumar, N. & Rotami, A. (2023). Exploring moisture content measurement using an open-ended coaxial sensor: A method of moments approach. Sensors and Actuators a Physical, 367, 114990.
https://doi.org/10.1016/j.sna.2023.114990

Suhaime, N. B. (2018). Open-ended Coaxial Sensor for Determination of Moisture Content, Soluble Solid Content, pH and Dielectric Properties of Chok Anan Mango (MSc dissertation, University Putra, Malaysia)

Sutthaweekul, R. (2019). Microwave NDT&E using open-ended waveguide probe for multilayered structures (Doctoral dissertation, Newcastle University).

Xu, Y., Bosisio, R., & Bose, T. (1991). Some calculation methods and universal diagrams for measurement of dielectric constants using open-ended coaxial probes. IEE Proceedings H Microwaves Antennas and Propagation, 138(4), 356.
https://doi.org/10.1049/ip-h-2.1991.0058

Yahya, N., Sikiru, S., Rostami, A., Soleimani, H., Shafie, A., Alqasem, B., Qureishi, S., & Ganeson, M. (2020). Percolation threshold of multiwall carbon nanotube-PVDF composite for electromagnetic wave propagation. Nano Express, 1(1), 010060.
https://doi.org/10.1088/2632-959x/ab9d69

Yusuf, J. Y., Soleimani, H., Yahya, N., Sanusi, Y. K., Adebayo, L. L., Sikiru, S., & Wahaab, F. A. (2020). Recent advances and prospect of cobalt based microwave absorbing materials. Ceramics International, 46(17), 26466–26485.
https://doi.org/10.1016/j.ceramint.2020.07.244

Yusuf, J. Y., Soleimani, H., Yahya, N., Sanusi, Y. K., Kozlowski, G., Öchsner, A., Adebayo, L. L., Wahaab, F. A., Sikiru, S., & Balogun, B. B. (2021). Electromagnetic wave absorption of coconut fiber-derived porous activated carbon. Boletín De La Sociedad Española De Cerámica Y Vidrio, 61(5), 417–427.
https://doi.org/10.1016/j.bsecv.2021.02.003